TU Delft

Delft University of Technology

Document Version
Final published version

Licence
Dutch Copyright Act (Article 25fa)

Citation (APA)
Bergmann, O. J., Van Zeijl, H. W., Van Driel, W. D., Qi Zhang, G., & Poelma, R. H. (2026). Compact Thermal Model of a Multi Die Power Stage with In-Package Sensing for Remaining Useful Life Prediction. In *Proceedings - 2026 27th International Conference on Thermal, Mechanical and Multi-Physics Simulation and Experiments in Microelectronics and Microsystems, EuroSimE 2026* (Proceedings - 2026 27th International Conference on Thermal, Mechanical and Multi-Physics Simulation and Experiments in Microelectronics and Microsystems, EuroSimE 2026). IEEE. https://doi.org/10.1109/EuroSimE69483.2026.11511981

Important note
To cite this publication, please use the final published version (if applicable).
Please check the document version above.

Copyright
In case the licence states “Dutch Copyright Act (Article 25fa)”, this publication was made available Green Open Access via the TU Delft Institutional Repository pursuant to Dutch Copyright Act (Article 25fa, the Taverne amendment). This provision does not affect copyright ownership.
Unless copyright is transferred by contract or statute, it remains with the copyright holder.

Sharing and reuse
Other than for strictly personal use, it is not permitted to download, forward or distribute the text or part of it, without the consent of the author(s) and/or copyright holder(s), unless the work is under an open content license such as Creative Commons.

Takedown policy
Please contact us and provide details if you believe this document breaches copyrights.
We will remove access to the work immediately and investigate your claim.

This work is downloaded from Delft University of Technology.

2026 27th International Conference on Thermal, Mechanical and Multi-Physics Simulation and Experiments in Microelectronics and Microsystems (EuroSimE) | 979-8-3315-6249-6/26/$31.00 ©2026 IEEE | DOI: 10.1109/EuroSimE69483.2026.11511981

Compact Thermal Model of a Multi Die Power Stage with In-Package Sensing for Remaining Useful Life Prediction

1st Ole J. Bergmann
Department of Microelectronics
Delft University of Technology
Delft, The Netherlands
o.bergmann@tudelft.nl

2nd Henk W. van Zeijl
Department of Microelectronics
Delft University of Technology
Delft, The Netherlands
h.w.vanzeijl@tudelft.nl

3rd Willem D. van Driel
Department of Microelectronics
Delft University of Technology
Delft, The Netherlands
willem.vandriel@tudelft.nl

4th Guo Qi Zhang
Department of Microelectronics
Delft University of Technology
Delft, The Netherlands
g.q.zhang@tudelft.nl

5th René H. Poelma
Department of Microelectronics
Delft University of Technology
Delft, The Netherlands
r.h.poelma@tudelft.nl

***Abstract*—The paper presents a degradation for remaining useful lifetime framework for smart power stages (SPS) with an integrated temperature sensor for electronic control units (ECU). A reduced order state space model with physically meaningful time constants is derived from finite element simulations. The state space model is the core of the damage estimation of the SPS during operation. A framework for remaining useful lifetime estimation is presented simulating degradation based on an estimated mission profile for cars. Temperature cycles are extracted and used to estimate the time constant drift representing package degradation. An exemplary approach on how to integrate degradation monitoring into a lifetime approximation of the package is presented. The state space model is extended for estimator based predictions to integrate the model in future test benches for real life monitoring and remaining useful life predictions of active devices.**

***Index Terms*—Multi-Die package, thermal state space model, smart power stage (SPS), time constant drift, remaining useful life (RUL)**

I. Introduction

Automotive electronic control units (ECU) for self-driving vehicles, are becoming a high-compute "brain" that runs safety-critical perception and control in real time. It must not freeze or behave unpredictably because of overheating, a short circuit, or a voltage dip. This makes power delivery and thermal behaviour an integral part of the safety concept.

Smart power stages (SPS) are in the power path and in close proximity to the ECU's central or graphics processing unit's (CPU/GPU) rails. The SPS operates as a buck-converter configuration experiencing high electrical and thermal stress. Cooling issues can occur in real life: restricted coolant flow, degraded thermal interface material (TIM), high ambient temperatures, or poor heat-sink contact. Temperatures can rise fast; electrical failures can arise even faster. Hardware protection is therefore essential part of system safety considerations.

Because our SPS contains accurate on-chip current and temperature sensing, as well as built-in protection capabilities it becomes an interesting component for safe system design. Furthermore, it provides real telemetry from the hottest and fastest location in the power delivery path, which is not only useful for protection, but also for monitoring, trend detection, and reliability concepts such as remaining useful life (RUL). However, to use these signals correctly, an accurate thermal model is required.

The SPS package studied in this paper is an advanced multi-die clip-bonded device with three thermal nodes of interest: a high-side (HS) MOSFET die, a low-side (LS) MOSFET die, and a gate-driver integrated circuit (GD-IC) featuring a temperature sensor. The metal-oxide-semiconductor-field-effect transistors (MOSFETs) are arranged in a half-bridge configuration posing a non-trivial thermal problem: the thermal coupling between the dies is significant and single die temperatures are can not be measured by the temperature sensor. Instead, it measures a coupled response that depends on where the heat is generated and how it spreads through the highly unsymmetrical package.

The three dies are assembled on three different copper pads, the source of the HS-MOSFET is connected via a copper clip with the drain of the LS-MOSFET and the switching output pin; the relevant blocks are shown in Fig. 1. All three dies in close proximity to each other on individual copper pads and not one copper base-plate make the biggest distinction to thermal analyses of multi-die power modules.

Compact thermal models for multi-die power modules have

This work has been supported by European public funding via Xecs by the NL ministry EZK under the reference XECS221003 in context of the e2LEAD project. Xecs is part of the EUREKA Clusters.

979-8-3315-6249-6/26/$31.00 ©2026 IEEE
Authorized licensed use limited to: TU Delft Library. Downloaded on July 14,2026 at 11:25:50 UTC from IEEE Xplore. Restrictions apply.

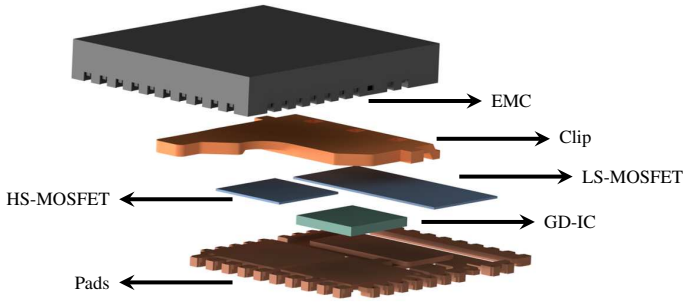
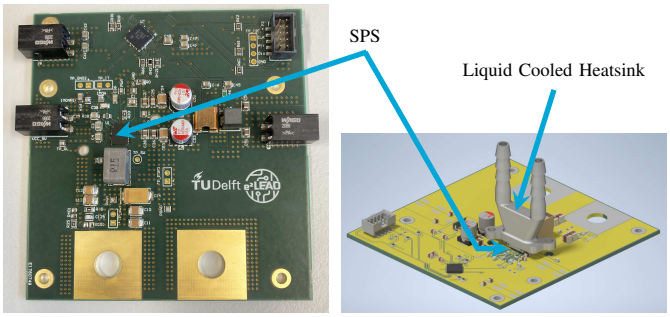


Fig. 1: Multi-Die package of a smart power stage (SPS).



(a) (b)

Fig. 2: (a) SPS degradation test platform and (b) CAD model of test PCB with liquid cooled heat-sink for ECU relevant conditions.

been developed and investigated in the past with accurate results [1], [2]. However, due to the architecture and primarily one-dimensional heat-flow with weak coupling due to big die-to-die distances, thermal coupling can be modelled with discrete RC networks. Thermal coupling in the SPS package is fully three-dimensional with strong coupling in two lateral directions and comprises the clip, the PCB, and the epoxy mold compound (EMC). The primary cooling path is the third dimension of heat-flow through the top of the package. The cooling path can thus not be entirely separated from the coupling.

This paper derives and validates a compact thermal model that captures this coupling. We investigate a compact thermal model for the three-die SPS, including the cross-coupling between dies and the sensor. The goal is a model that is accurate enough for two practical uses: (1) estimating the MOSFET junction temperatures from the IC sensor temperature during real operation, and (2) translating mission profiles into realistic thermal stress metrics that can feed lifetime and RUL estimation.

To evaluate this in an ECU-relevant setup, we integrate the SPS in a buck-converter configuration on a dedicated ($89\,\mathrm{mm}$ by $84.5\,\mathrm{mm}$) PCB as shown in Fig. 2(a). We are reproducing tight thermal environmental conditions by attaching a compact liquid-cooled heat sink to the top of the package (Fig.2(b)).

TABLE I: PCB model with material properties at room temperature.

Material-Layer	λ **[W/mK]**	c_p **[J/kgK]**	ρ **[kg/m^3]**	t **[mm]**
1 - Copper	388	382	8938	0.035
2 - FR-4	0.45	920	2000	0.24
3 - PCB material	42	865	2715	1.34
4 - Copper	388	382	8938	0.035

II. Methodology

This section describes the derivation of a reduced order model (ROM) to estimate the junction temperatures of the MOSFETs based on the read-out from the temperature sensor First, a transient thermal simulation is performed to extract the coupling between dies by means of a thermal impedance matrix as has been done several times before [3], [4]. Subsequently, appropriate time constants are extracted to represent the thermal impedances by a set of weighted kernel functions. Lastly, a state-space representation to describe the thermal system is derived featuring the time constants and weighting factors for physical significance.

A. Model Setup

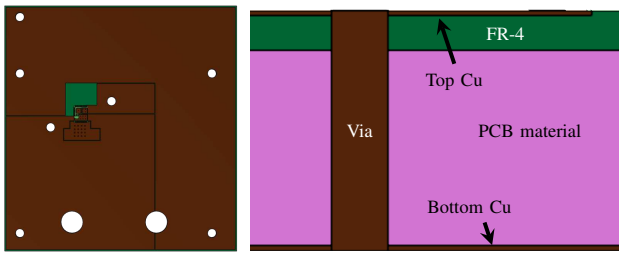
For the simulation, the use case as described in the previous section is chosen as a reference. Therefore, the boundary conditions and model build up follow the design of the PCB and heat-sink described above.

For the following finite element method (FEM) simulation COMSOL Multiphysics® software is used. For the materials of the package, standard built-in materials are used for epoxy molding compound (EMC), the silicon dies (HS/LS-MOSFET, GD-IC), UNS copper for the clip and pads, AgSn solder for the solder joints between the dies and the clip and the dies and the pads. Soldering between the package and the PCB as well as the wire bonds connecting the GD-IC are neglected in the model.

All peripheral components are neglected for the simulation and the PCB is simplified to four layers with the specifications as shown in Table I. Thereby the properties of the PCB material are computed by the relative proportions of the FR-4 and copper in the stack and their material properties, respectively. Copper vias from the PCB solder pads ($\varnothing = 200\,\mu\mathrm{m}$) and on the output plane ($\varnothing = 400\,\mu\mathrm{m}$) on the PCB to the bottom copper layer are respected in the FEM model and added to the geometry. The cross-section of the PCB at the edge is shown in Fig 3(a), the top copper plane is recessed in the FR-4 layer. For the sake of simplicity, the top copper layer is simplified in the simulation as shown in Fig. 3(b) to reduce simulation time but the different copper areas that are in contact with the pads of the package are kept separate.

As mentioned in the introduction, the configuration is inspired by applications scenarios in a closed case with active cooling from the top as e.g, in an ECU. Therefore, the boundary conditions for the simulation are defined as thermally insulating to all sides except the topside of the package. A thermal interface material (TIM) with a thermal conductivity of $\lambda = 5\,\mathrm{W/mK}$ and a thickness of $t = 500\,\mu\mathrm{m}$ is added between the top of the package and the aluminium heatsink

Authorized licensed use limited to: TU Delft Library. Downloaded on July 14,2026 at 11:25:50 UTC from IEEE Xplore. Restrictions apply.



(a) (b)

Fig. 3: (a) Top side copper area for simulated PCB and (b) cross-section of the PCB model.

that is modelled as a $2\,\mathrm{mm}$ thick aluminium block with a boundary condition of a constant $25\,^{\circ}\mathrm{C}$.

B. Transient Simulation

To extract the coupling between the HS die, the LS die and the temperature sensor in the GD-IC die, two transient thermal simulations are run with a $1\,\mathrm{W}$ power step in the HS and LS from $700\,\mathrm{ns}$ to $40\,000\,\mathrm{s}$, respectively. The power dissipation in the GD-IC is smaller than the dissipated power in the MOSFETs by magnitudes and can therefore be neglected.

The thermal impedances from the HS-MOSFET, LS-MOSFET, and the sensor can then be calculated by subtracting the ambient temperature from the temperature of the respective node. This yields six thermal impedances of the node j with respect to the active junction i:

$$Z_{ij}(t), \quad i \in \{\mathrm{HS}, \mathrm{LS}\}, \quad j \in \{\mathrm{HS}, \mathrm{LS}, \mathrm{IC}\}, \tag{1}$$

where $\{Z_{ij}(t) : i = j\}$ are the two junction-to-ambient thermal resistances and the thermal system with the relevant temperatures on the high side, low side and the temperature sensor (T_j) can be described by:

$$\begin{pmatrix} T_{\mathrm{HS}} \\ T_{\mathrm{LS}} \\ T_{\mathrm{IC}} \end{pmatrix} = \begin{pmatrix} Z_{\mathrm{HS,HS}} & Z_{\mathrm{LS,HS}} \\ Z_{\mathrm{HS,LS}} & Z_{\mathrm{LS,LS}} \\ Z_{\mathrm{HS,IC}} & Z_{\mathrm{LC,IC}} \end{pmatrix} \times \begin{pmatrix} P_{\mathrm{HS}} \\ P_{\mathrm{LS}} \end{pmatrix} + \boldsymbol{T}_{\mathrm{a}}, \tag{2}$$

With the power dissipations (P_i) at the high side and low side junction, respectively and the reference or starting temperature $\boldsymbol{T}_{\mathrm{a}}$.

C. Thermal Modes Extraction

With the thermal impedances extracted from the simulation the reduced order model (ROM) is derived with the following steps:

1) Fitting global time constants τ to characteristic impedance functions (kernels) to represent transient behaviour of all thermal impedances by one set of common τ.
2) Fit weights to approximate all thermal impedances by kernels and weights only.
3) Split mode with largest relative error to improve spatial resolution.

In the first step, $K = 4$ time constants τ_x are uniformly distributed over the transient period between power step input and steady state. The gap between neighbouring τ is set to be smaller than 2.2 decades, to achieve a sufficient coverage over the entire timespan.

Once the initial time constants are set, they are refined and further fitted to constitute all six thermal impedance curves with one set. This is done by minimizing a cost function defined as the sum of squared error (SSE). The linear combination of k weighted kernels

$$\Phi_k(t) = 1 - \exp(-t/\tau_k) \tag{3}$$

yields a shared set $\{\tau_k\}_{k=1}^{K}$ which represents the transient behaviour of all six thermal impedances.

The weights for the linear combination of kernels are computed by a non-negative least squares algorithm to the log-time compensated thermal impedances. The thermal impedances are compensated by coefficients to prevent biasing of late times and ignoring early time constants. The fitted thermal impedances ($Z'_{ij}(t)$) can now be described by:

$$\begin{pmatrix} Z'_{\mathrm{HS,HS}}(t) & Z'_{\mathrm{LS,HS}}(t) \\ Z'_{\mathrm{HS,LS}}(t) & Z'_{\mathrm{LS,LS}}(t) \\ Z'_{\mathrm{HS,IC}}(t) & Z'_{\mathrm{LC,IC}}(t) \end{pmatrix} = \sum_{k=1}^{K} \Phi_k(t) \times \boldsymbol{W}_k \tag{4}$$

with a weight matrix for each kernel of the form:

$$\boldsymbol{W}_k = \begin{pmatrix} w_{11k} & w_{12k} \\ w_{21k} & w_{22k} \\ w_{31k} & w_{32k} \end{pmatrix}. \tag{5}$$

With this approach we can express the thermal impedances by weighted kernel functions with different time constants. Each time constant contains a physical meaning of the package structure. Fast, i.e., small time constants represent temperature changes close to the junction, i.e., the die and die-attach region. Medium time constants provide information about the clip and package response, and large time constants about the influence of the PCB or thermal interface material (TIM).

D. Model Enhancement through Mode Splitting

Based on the previously derived weights, we are now seeking the relations between

I. the inputs (P_i) and the thermal modes, and
II. the thermal modes and the output temperatures (T_j).

To achieve this, the weights are factorized in an input pattern $\tilde{\boldsymbol{B}}_{\mathrm{inp}}$ to capture (I), and an output pattern $\tilde{\boldsymbol{C}}$ to capture (II). The matrices $\tilde{\boldsymbol{B}}_{\mathrm{inp}}$ and $\tilde{\boldsymbol{C}}$ can be derived by non-negative factorization of each matrix $\boldsymbol{W}_k$ such that:

$$\hat{\boldsymbol{W}} = \tilde{\boldsymbol{C}} \times \tilde{\boldsymbol{B}}_{\mathrm{inp}} = \begin{pmatrix} | & | & | & | \\ \boldsymbol{c}_1 & \boldsymbol{c}_2 & \boldsymbol{c}_3 & \boldsymbol{c}_4 \\ | & | & | & | \end{pmatrix} \times \begin{pmatrix} \mathbf{b}_1^{\top} \\ \mathbf{b}_2^{\top} \\ \mathbf{b}_3^{\top} \\ \mathbf{b}_4^{\top} \end{pmatrix}. \tag{6}$$

Due to the asymmetries in the package, e.g. the different HS and LS size and asymmetric placement, i.e., the IC placed at different relative positions to the HS and LS MOSFET, and

Authorized licensed use limited to: TU Delft Library. Downloaded on July 14,2026 at 11:25:50 UTC from IEEE Xplore. Restrictions apply.

the asymmetric shaped clip, one of the modes is split and represented by spatial heat patterns.

The mode with the largest relative error between $\boldsymbol{W}_k$ and $\hat{\boldsymbol{W}}_k$ is split, as this mode is not sufficiently represented by only one spatial pattern. In this case it was found that the mode with the largest error is the first mode representing τ_1 and can physically be interpreted as heat spreading and temperature in vicinity to the junction varies on the HS and the LS. Therefore the first mode is split and factorized with a second rank as:

$$\hat{\boldsymbol{W}}_1 = \boldsymbol{c}_{1a} \otimes \boldsymbol{b}_{1a} + \boldsymbol{c}_{1b} \otimes \boldsymbol{b}_{1b}. \tag{7}$$

Adding the split modes to the factorization matrices $\tilde{\boldsymbol{B}}_{\text{inp}}$ and $\tilde{\boldsymbol{C}}$ yield the final input

$$\boldsymbol{B}_{\text{inp}} = \begin{pmatrix} \mathbf{b}_{1a}^\top \\ \mathbf{b}_{1b}^\top \\ \mathbf{b}_2^\top \\ \mathbf{b}_3^\top \\ \mathbf{b}_4^\top \end{pmatrix}, \tag{8}$$

and output pattern

$$\boldsymbol{C} = \begin{pmatrix} | & | & | & | & | \\ \boldsymbol{c}_{1a} & \boldsymbol{c}_{1b} & \boldsymbol{c}_2 & \boldsymbol{c}_3 & \boldsymbol{c}_4 \\ | & | & | & | & | \end{pmatrix}. \tag{9}$$

E. State Space Model

The heat-flow through each thermal mode x_k with their time constant τ_k can be described with an ordinary differential equation of the form

$$\dot{x}_k(t) = -\frac{1}{\tau_k} x_k(t) + \frac{1}{\tau_k} \sum_i \boldsymbol{B}_{\text{inp},ki} \boldsymbol{P}_i(t), \tag{10}$$

because the step response of

$$\dot{x}_k = -\frac{1}{\tau_k} x_k + \frac{1}{\tau_k} u_k \tag{11}$$

is the thermal impedance kernel Φ_k [5]. Therefore, the entire thermal system of the package can be expressed in state-space notation [6] with the derived parameters as:

$$\dot{\boldsymbol{x}}(t) = \boldsymbol{A}\boldsymbol{x}(t) + \boldsymbol{B}\boldsymbol{P}(t) \tag{12}$$

$$\boldsymbol{T}(t) = \boldsymbol{C}\boldsymbol{x}(t), \tag{13}$$

where

$$\boldsymbol{A} = \begin{pmatrix} -1/\tau_1 & 0 & 0 & 0 & 0 \\ 0 & -1/\tau_1 & 0 & 0 & 0 \\ 0 & 0 & -1/\tau_2 & 0 & 0 \\ 0 & 0 & 0 & -1/\tau_3 & 0 \\ 0 & 0 & 0 & 0 & -1/\tau_4 \end{pmatrix} \tag{14}$$

and

$$\boldsymbol{B} = -\boldsymbol{A} \times \boldsymbol{B}_{\text{inp}}. \tag{15}$$

The state-space model combines the previous derived assumptions and simplifications into a compact model. It can be used to model the dynamic thermal system with an arbitrary temporal resolution and arbitrary input powers. It is based on the physics of the system analogous to the Cauer RC network representation.

The resulting thermal impedance curves for the FEM simulated thermal impedance, the kernel fit with $K = 4$ thermal modes and the shared-mode-state model fit are shown in Fig. 4(a) for a P_{HS} step input and in Fig. 4(b) for a P_{LS} step input, respectively.

F. Model Validation

The model was derived based on the simulation with unit step inputs of each junction at a time (HS or LS). In real operation, the MOSFETs are switched at a frequency of several $100\,\text{kHz}$ which is orders of magnitude faster than the smallest thermal time constant identified. Therefore, the model assumes time averaged power dissipations in each junction present at the same time. Hence, for validation, the model must demonstrate that its forward calculated temperatures T_j ($j \in \{\text{HS}, \text{LS}, \text{IC}\}$) remain accurate for arbitrary simultaneous power inputs of both junctions.

The validation dataset contains a sequence of different power input levels in both junctions. The datasets tests whether the assumption of superposition of the derived mode patterns holds for simultaneous power dissipations in both junctions. The model is used in an open loop configuration during validation and not corrected. The state-space model computes the temperatures at the same output time instances as the FEM simulated model. Fig. 5 compares the temperatures modelled in COMSOL with the temperatures computed by the share-mode state space model. Fig. 6 provides more detail on the transient response until the first steady state. The shared-mode state space model reproduces the transient dynamics over several decades.

The absolute total error of the state-space computed temperature is $< 1.5\,^\circ\text{C}$. The relative error is well within an interval of $\pm 2.5\,\%$ even during transients which shows that the set of shared time constants $\{\tau_k\}$ captures the physical thermal mass distribution of the package. This is true for rising as well as falling edges. The model therefore confirms the underlying assumption of linearity and superposition in the share-mode state space formulation while being more compact than conventional RC network models making it suitable for integration in control and diagnostic monitoring frameworks. It is the core for the investigation in the next section where it is used further extended for estimator design and lifetime assessments.

III. Remaining Useful Life

Thermal paths in multi-die power packages degrade with use, i,e, temperature cycles. Clip interfaces, die attach, and the board/heat-sink stack can all change their effective thermal resistance and capacitance over life. In practice, we often only observe a shift in a measured thermal response, without knowing which physical region is responsible. This uncertainty complicates root-cause analysis and makes it hard to translate thermal monitoring into remaining useful lifetime (RUL) estimates. A compact, physics-guided model that can both

Authorized licensed use limited to: TU Delft Library. Downloaded on July 14,2026 at 11:25:50 UTC from IEEE Xplore. Restrictions apply.

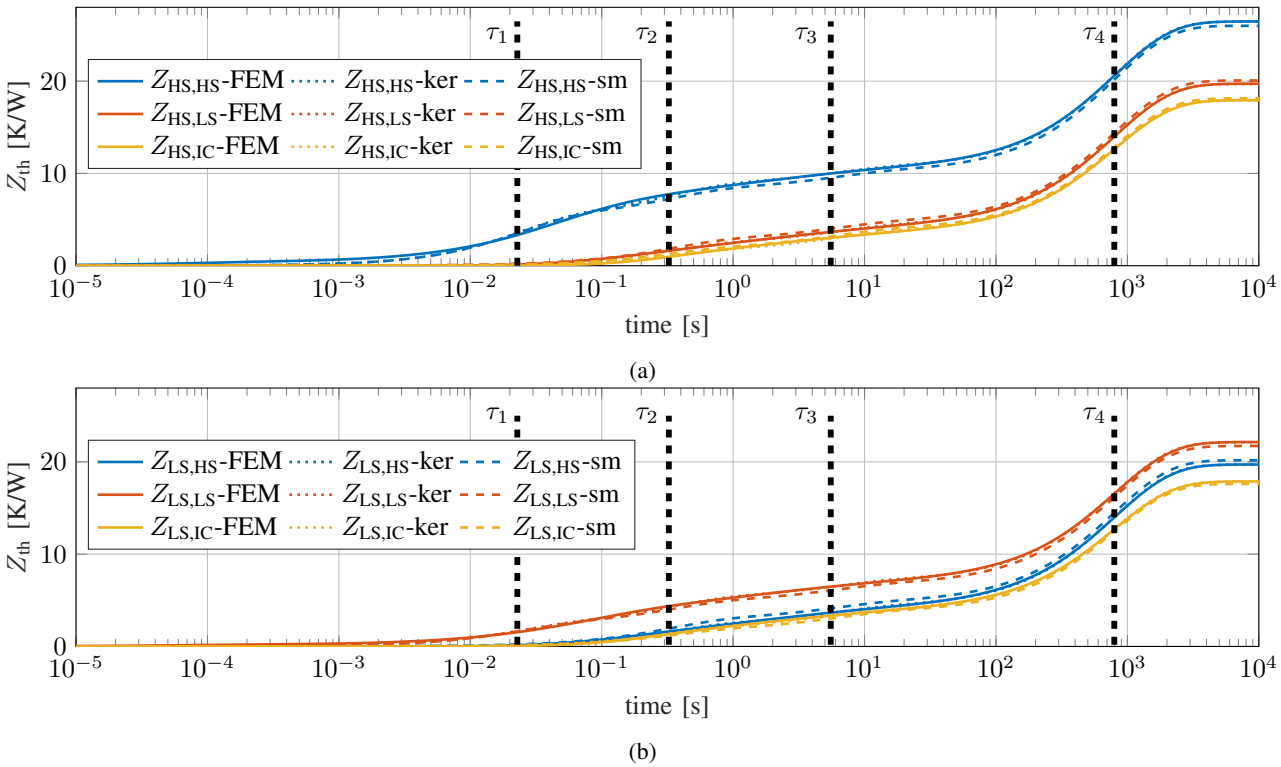


Fig. 4: Thermal impedance curves for HS step input FEM simulated (FEM), kernel fitted (ker), and share-mode-state-space (sm) fitted for (a) HS and (b) LS step input.

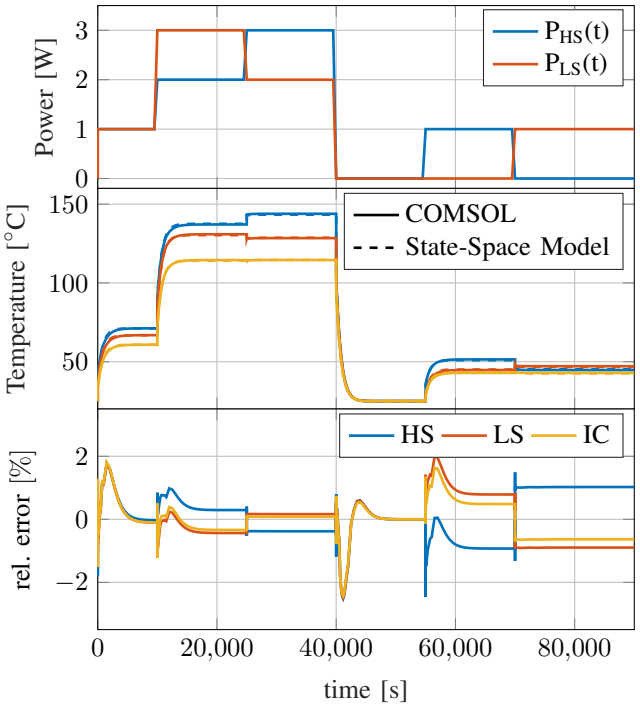


Fig. 5: Shared-mode state-space model validation with simultaneous arbitrary input powers and relative error.

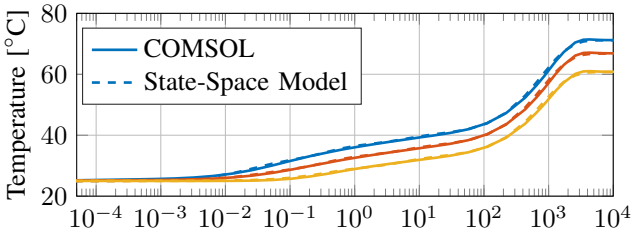


Fig. 6: Transient input response for 1 W at HS and LS.

(i) predict junction and sensor temperatures and (ii) localize which heat path is drifting is therefore valuable for reliability engineering and condition monitoring.

Our model represents a package with a small number of thermal modes. Each mode corresponds to a heat-affected region (local die/die attach, clip/leadframe and mold/PCB, TIM/heat-sink) and is characterized at a single thermal time constant, which are captured in a state-vector. Because the model is built from first order modes, it remains computationally light and physics guided.

The purpose of the model developed in the previous chapter is to serve as a diagnostics tool for lifetime and remaining useful life (RUL) assessments and predictions based on real-time sensor data [7]. The key for achieving this is the enhancement of the shared-mode state space model from computing the die temperatures based on the power dissipated in the junctions towards the estimation of the junction temperatures based on

Authorized licensed use limited to: TU Delft Library. Downloaded on July 14,2026 at 11:25:50 UTC from IEEE Xplore. Restrictions apply.

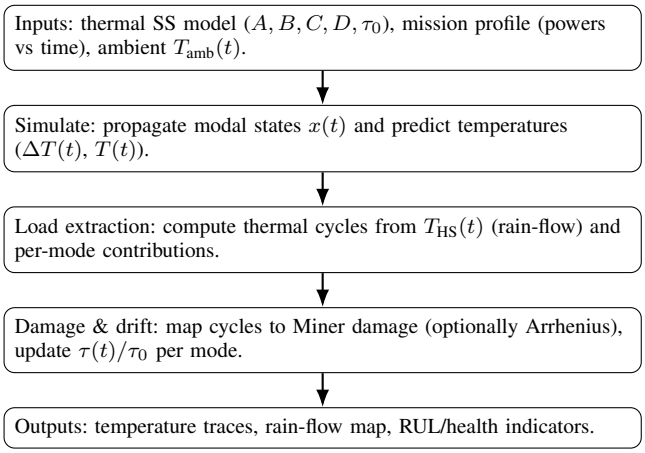


Fig. 7: Compact workflow of the thermal-model-based degradation and RUL estimation.

the temperature sensor, i.e. T_{IC}, data. The methodology from model input to degradation outputs are summarized in the flowchart in Fig. 7 and each step explained in the following sections.

Because the time constants τ_k have a physical meaning, degradation appears as a change of the transient response and thus a shift in time constants which are used as degradation indicators. A time constant increase indicates a slower heat transport path, this is consistent with a degraded interface or reduced heat transfer.

To show the applicability of this method, real sensor data is required which is beyond the scope of this paper. Instead, a scenario simulating the use of the SPS in a car ECU is provided for demonstration purpose. The scenario includes the following features:

I. The car is assumed to follow a mission including daily morning and evening commutes. On some weekdays, short grocery trips follow the usual evening commute; weekends include occasional extended trips. The length of each trip is dependent on a base duration of $45\,\text{min}$ for commutes, $12\,\text{min}$ for groceries, and $180\,\text{min}$ for weekend trips, respectively. Additionally, all trips have a randomized portion for the starting time each day and the total length.

II. Intra-day and seasonal ambient temperature variations. The ambient temperature varies following a sinusoid over one year representing the seasons super positioned with a daily sinusoidal variation representing day and night cycles. The day to day variation also feature a random portion. Once a year, heat waves and freeze periods occur for several days causing extreme ambient temperatures and triggering traffic jams extending the daily commute times (extreme events).

III. The power dissipation is zero when the car is not used, and follows a constant dissipation during use. The power dissipation in the HS MOSFET is however assumed to be higher than in the LS MOSFET.

A. Damage Estimation

At the end of every simulated day, the time dependent HS junction temperature $T_{\text{HS}}(t)$ are evaluated for maximum temperature swing ΔT, mean temperature T_{mean} and number of temperature cycles N_{R} following a rainflow counting algorithm [8]. The cycles to failure are computed for each temperature mode based on the temperature swing at the HS MOSFET. For now, the degradation model follows a Coffin-Manson approach where the number of cycles to failure for each mode k is a function the temperature swing which is calculated and updated after every day following:

$$N_{\text{f}}^{(k)} = N_{\text{ref},k}\left(\frac{\Delta T_{\text{ref}}}{\Delta T}\right)^{m_{\text{CM}}}. \tag{16}$$

Here, the reference temperature and Coffin-Manson exponent are chosen as $\Delta T_{\text{ref}} = 20\,^{\circ}\text{C}$ and $m_{\text{CM}} = 5$, respectively. The reference number of cycles are highly approximative at this stage and can be subject to further research. The damage increment ΔD_k is monitored daily with

$$\Delta D_k = \sum_m \frac{c_m}{N_{\mathbf{f}}^{(k)}(\Delta T_i)}, \tag{17}$$

where c_m indicates either a half cycle ($c_m = 0.5$) or a full cycle ($c_m = 1$) count in the rainflow counting algorithm. ΔD_k is added to the accumulated lifetime damage D_k, the maximum lifetime damage is 1.

B. Time Constant Drift

For the theoretical trial and proof of concept in this investigation the time constants are altered purely by the ideal simulated junction temperatures using the forward shared-mode state space model based on power dissipations. At the end of every day the time constants in the state space model are updated after being degraded according to the damage model which is explained in the following section. The degradation of each time constant is a function of the accumulated damage D_k and is described by

$$\tau_k(D_k) = \tau_{k,0}[1 + (AF_{\text{EOL}} - 1)D_k] \tag{18}$$

with the initial time constant $\tau_{k,0}$ and the end-of-life amplification factor AF_{EOL} which is set to 1.3 in analogy to common assumptions of R_{th} degradation thresholds [9], [10].

C. Remaining Useful Life Prediction

The end-of-life amplification factor defines the criterion for the component end-of-life (EOL). As mentioned above, the end-of-life condition is reached when one of the time constants increases by $30\,\%$. The remaining margin until the EOL is reached can be derived using (18) and the end-of-life criterion:

$$\max_k \frac{\tau_k}{\tau_{k,0}} = AF_{\text{EOL}} \Rightarrow \max_k D_k = 1.$$

We can now choose a conservative approach to extrapolate the time until failure linearly by using the accumulated damage of

Authorized licensed use limited to: TU Delft Library. Downloaded on July 14,2026 at 11:25:50 UTC from IEEE Xplore. Restrictions apply.

the dominant ageing mode ($\max_k D_k$) and monitor the average degradation per day:

$$\text{RUL} \approx \frac{1 - \max_k D_k}{\max_k(\Delta D_k)}. \tag{19}$$

Accumulated degradation causing inferior thermal performance over the lifetime of the device is respected in this approach as it is updated after each day taking the increased temperature swings into account. Extreme events such as heatwaves are immediately reflected in the estimated RUL.

In an operational system, the junction temperature data is predicted using an estimator from the temperature sensor readout as addressed in the next section.

D. Extending State-Space Model with Estimator

Since the temperature sensor can be utilized during operation, the prediction of the sensor temperature is not crucial for the monitoring aspect but can be compared to the actual measured temperature to detect baseline deviations. The initial estimation of the change of heatflow in each node $\hat{x}_k$ remains the same following (12). Subsequently, the expected sensor temperature based on the computed $\hat{\boldsymbol{x}}_{n+1|n}$ is derived using only the row of (13) relevant to the sensor. We then use a Kalman filter to correct the initial estimation $\hat{\boldsymbol{x}}_n$ by a Kalman gain and the difference between the expected sensor temperature and the measured sensor temperature and get the corrected state vector $\boldsymbol{x}$ [11]. For this theoretical demonstration we assume a sensor noise variance of $0.1\,\%$ and a process noise intensity of $1\,\text{ppm}$. With this corrected state vector the expected junction temperatures can be derived using (13). This aspect of the model becomes important when the model is deployed to validation with real components.

IV. Results

The simulation of a model under an estimated and arbitrarily generated real world mission profile for 5 years was run. For demonstration purpose and to see effects after short time spans, a scale factor for damage amplification is used. The daily ambient temperature and driving time underlying for the simulation are shown in Fig. 8. The cumulative rain-flow diagram in Fig. 10 shows the accumulated damage of the dominant ageing mode (colour grading) as a function of temperature cycle count (z-axis), temperature swing per cycle, and the mean temperature per cycle. The temperature swing and temperature cycles are summarized in intervals of $10\,^\circ\text{C}$. From the rain-flow diagram clearly shows that cycles with large temperature swings have a more severe effect on the health-state of the device than smaller temperature swings as, e.g. induced by daily ambient temperature variations. Fig. 9 shows the time constant shift over the simulated time and the decreasing RUL estimate. The RUL estimate in this simulation is based on the dominant ageing mode with a Coffin-Manson degradation model to showcase how lifetime estimations could be derived from live temperature cycling data. The damage scale factor chosen for the simulation causes a noisy RUL prediction with uncertainties of some years. However, a clear trend in decaying RUL is apparent.

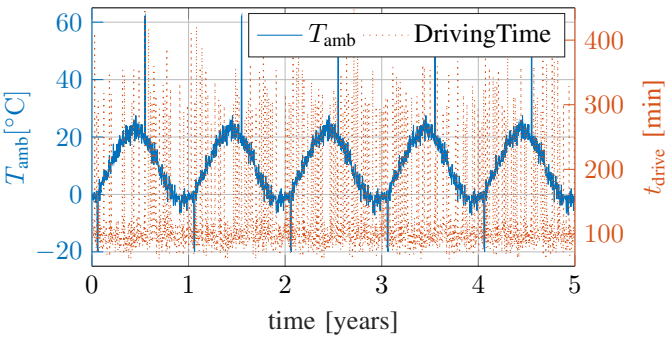


Fig. 8: Daily ambient temperature and driving time.

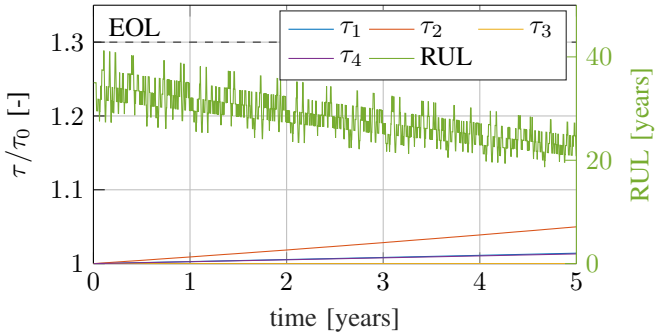


Fig. 9: Time constant drift and RUL estimate.

V. Conclusion and Outlook

This paper demonstrates how a space-model for a smart power stage based on physically meaningful time constants is derived. The methodology is based on a kernel fit of the thermal impedance matrix which is extracted from FEM simulations. The fit of the state space model was validated with a relative error $< 2.5\%$. The model is capable to capture the transient dynamics of the device accurately which makes it suitable for lifetime monitoring through time constant drift. The model was successfully integrated in a basic damage estimation framework based on a rain-flow counting algorithm and time constant drift. The remaining useful lifetime was estimated by extrapolation of the accumulated degradation of the dominant ageing mode until the end-of-life criterion is

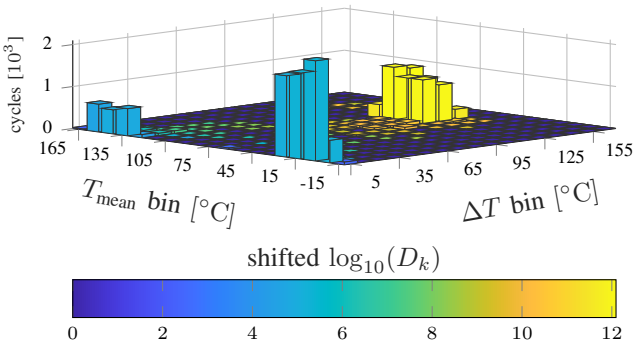


Fig. 10: Accumulated damage as function of cycles and temperature from rain-flow counting.

Authorized licensed use limited to: TU Delft Library. Downloaded on July 14,2026 at 11:25:50 UTC from IEEE Xplore. Restrictions apply.

reached.

The presented demonstration of the degradation model provides a comprehensive simulation for remaining useful lifetime prediction and a framework for future application tests. However, the here used Coffin-Manson estimation might not be a valid model for all time-constants and different degradation models might be used to estimate the degradation of different time constants. Future work will focus on running the presented RUL model with an estimator driven state-space model taking the next step towards real life coupling of model and device towards functional validation. The next steps towards integration in a real ECU comprise model validation with real world sensor data. A test bench for stress and reliability tests is currently prepared to use the model as a digital twin.

ACKNOWLEDGEMENT

The authors thank Kasia Nowak, Sambhav Jain, Jizhe Yin, Sooraj Nair and Sven Walczyk from Nexperia for the project support, access to facilities and fruitful discussion boosting ideas. Furthermore the project partners in the e2LEAD project for critical and ingenious exchanges refining ideas and scopes of the work presented.

REFERENCES

[1] A. S. Bahman, K. Ma, and F. Blaabjerg, "A lumped thermal model including thermal coupling and thermal boundary conditions for high-power igbt modules," *IEEE Transactions on Power Electronics*, vol. 33, no. 3, pp. 2518–2530, 2018.

[2] J. Li, A. Castellazzi, M. A. Eleffendi *et al.*, "A physical rc network model for electrothermal analysis of a multichip sic power module," *IEEE Transactions on Power Electronics*, vol. 33, no. 3, pp. 2494–2508, 2018.

[3] A. Allegra, G. Scelba, M. Cacciato *et al.*, "Thermal equivalent circuit model of multi-die sic power modules," in *2020 ELEKTRO*, 2020, pp. 1–6.

[4] A. Poppe, Y. Zhang, G. Farkas *et al.*, "Thermal characterization of multi-die packages," 01 2007, pp. 500 – 505.

[5] D. Di Ruscio, "System theory state space analysis and control theory," Lecture, Control Theory, Systems and Control Engineering, University of South-Eastern Norway, Porsgrunn, Norway, 2022.

[6] K. Hangos, R. Lakner, and M. Gerzson, *Intelligent Control Systems: An Introduction with Examples*. Springer, 2004.

[7] X. Wang, A. Castellazzi, and P. Zanchetta, "Observer based temperature control for reduced thermal cycling in power electronic cooling," *Applied Thermal Engineering*, vol. 64, no. 1, pp. 10–18, 2014.

[8] *Standard Practices for Cycle Counting in Fatigue Analysis*, Std., 2023.

[9] W. Lai, M. Chen, L. Ran *et al.*, "Study on the lifetime characteristics of power modules under power cycling conditions," *IET Power Electronics*, vol. 9, no. 5, pp. 1045–1052, 2016.

[10] S. Baba, A. Gieraltowski, M. Jasinski *et al.*, "Active power cycling test bench for sic power mosfets—principles, design, and implementation," *IEEE Transactions on Power Electronics*, vol. 36, no. 3, pp. 2661–2675, 2021.

[11] B. Rodríguez, E. Sanjurjo, M. Tranchero *et al.*, "Thermal parameter and state estimation for digital twins of e-powertrain components," *IEEE Access*, vol. 9, pp. 97 384–97 400, 2021.

Authorized licensed use limited to: TU Delft Library. Downloaded on July 14,2026 at 11:25:50 UTC from IEEE Xplore. Restrictions apply.